# NUMERICAL STUDY OF VORTEX RING EVOLUTION AND INTERACTION WITH A FREE SURFACE

**Philip J. Archer, T. Glyn Thomas, Chris P. Yorke, Gary N. Coleman**
School of Engineering Sciences,
University of Southampton
Highfield, Southampton, Hampshire, SO17 1BJ, UK
pja@soton.ac.uk

## ABSTRACT

Direct Numerical Simulation (DNS) is used to evolve two initially laminar vortex rings, of differing core thickness, through transition to the turbulent regime. We investigate the vortical structure which defines the respective phases and give an account of the turbulent breakdown process. The structure of the resultant turbulent ring is found to be different for the thin- and thick-core rings. The thin-core ring maintains a coherent core structure whereas the thick-core becomes a swirling mass of vorticity filaments. Using the vorticity field as an initialisation, we investigate the surface interaction of vortex rings in a laminar, transitional and turbulent state. We find characteristic surface deformations and vorticity reconnections specific to the condition of the ring.

## INTRODUCTION

Vortex rings are interesting for a number of reasons, ranging from their ubiquitous nature to the fact that their growth, instability, and breakdown represent a prototypical turbulent flow. We focus here upon the structural development of a single ring during this breakdown process and its effect on a free surface.

The laminar vortex ring, typified by a toroidal core of vorticity, is unstable to azimuthal disturbances whose amplification distorts the core into a stationary azimuthal wave of wavenumber $m$ (Krutzsch, 1939). Maxworthy (1972, 1977), and Widnall & Sullivan (1973) showed experimentally that the wave grows in the conical surface at 45° to the axis of ring propagation. The rigorous mathematical treatment of Widnall & Tsai (1977) deduced an inviscid growth rate for the instability, to which a viscous correction was added by the DNS of Shariff *et al.* (1994). The vortex ring instability is an example of the elliptical instability, a review of which is given by Kerswell (2002).

The instability initially grows linearly, followed by a short transitional period featuring nonlinear wave growth, culminating in a turbulent vortex ring. The model decompositions from the numerical simulations of Shariff *et al.* (1994) and experiments of Dazin *et al.* (2006) show that the nonlinear phase is heralded by exponential growth of higher-order harmonics of the most unstable linear modes, followed by rapid growth of an $m = 0$ mode corresponding to a mean azimuthal velocity (also seen in the experiments of Naitoh *et al.* (2002)). Dazin *et al.* also reported the development of vortical structures on the (outer) periphery and interior of the ring, leading to ejection of vorticity into the wake. They inferred that the vortical structures were progressively wrapped around the core;. This is consistent with the vorticity tubes observed in the experiments of Schneider (1980) during the latter stages of transition. Recently Bergdorf *et al.* (2007) analysed the vortical structures numerically and suggested that they originate from locally stretched regions of the deformed vortex core.

The experiments of Wiegand & Gharib (1994) tracked vortex rings at an initial Reynolds number of 7500 (based on ring circulation $\Gamma$) through the laminar into the turbulent regime via the naturally occurring azimuthal instability. Their results for the turbulent phase of the ring evolution show that the ring maintains a definite coherent core structure with smaller scale vorticity regions in the periphery of the cores. A turbulent wake is generated behind the ring which consists of hairpin vortices, which are the remainder of the secondary vortical structure (Bergdorf *et al.*, 2007). The loss of organised structure leads to a 'staircase-like' decay in time of circulation and velocity, with the velocity lagging the circulation by a small amount. Glezer & Coles (1990) also noted the peripheral vortex structures, suggesting that their presence influences the local entrainment and detrainment dynamics. Weigand and Gharib found that the turbulent ring relaminarised when the loss of ring circulation decreased the Reynolds number below 2300.

We intend to determine the effect of the characteristic ring structure on the normal interaction of a vortex ring with a free surface. Song *et al.* (1992) investigated experimentally the normal interaction of laminar rings with a clean (surficants removed) surface. It was found that the approach of the ring is marked by an increase in diameter due to the influence of the virtual mirror image above the surface. This radial expansion is coupled with constriction of the core to preserve the continuity of vorticity lines. As the core propagates radially below the surface, the dynamics of the core and the local strain field are dominated by the image vortex above the surface. The ring locally approximates a pair of line vortices and the core is susceptible to the Crow instability (Crow, 1970), a long-wave example of the elliptical instability. This causes a wavy core structure to develop in the same 45° plane as the short-wave laminar instability. As the core waves grow in amplitude the core disconnects and reconnects with the free surface in a series of U-shaped hoops. Quyuan & Chu (1997) performed an inviscid simulation of the normal ring interaction with a deformable surface. They found that inviscid behaviour of the ring followed that of Song *et al.* but the vortex ring did not reconnect with the surface. This is not unexpected as surface reconnection is a viscous phenomenon (Ashurst & Meiron, 1987).

This paper is in two parts. In the first part, we present results from DNS of the unbounded vortex ring, concentrating on the evolution of the ring structure through the laminar, transitional and turbulent phases. In the second part, we perform a DNS of the normal interaction between vortex rings, at different stages of evolution, and a deformable free surface.

## NUMERICAL APPROACH

The numerical approach splits naturally into two steps: the precursor simulation of a vortex ring in an effectively unbounded domain, and the subsequent interaction of the developed ring with the free surface including the free surface dynamics. Each step is simulated with a different numerical code as described below.

### Unbounded Vortex Ring

The incompressible Navier-Stokes equations are discretized on a staggered cartesian grid using second-order finite differences in space with Adams-Bashforth stepping in time. Continuity is imposed using a standard pressure correction method and the resulting Poission equation for the pressure field is solved using a multigrid technique; see, for further details, Yao *et al.* (2001). The initial simulations showed that a significant wake is produced by the vortex ring during both the laminar and turbulent phases of its development, and so to avoid any interference from the wake we employ inflow and outflow boundary conditions in the direction the ring is traveling, i.e. along the $z$-axis, rather than the periodic conditions used in the other directions. Additionally, we keep the ring in the centre of the computational domain by performing the calculations in an (unsteady) moving reference frame attached to the ring, and adding a tracking system and controller to enforce this. It thus provides the propagation velocity of the vortex velocity $W_1(t)$ in a natural way and also defines inflow boundary condition at $z = +L_z/2$. The remaining velocity components satisfy the Neumann conditions $\partial u/\partial z = \partial v/\partial z = 0$ which are equivalent to enforcing a vanishing inlet vorticity. At the outflow plane $z = -L_z/2$ all three components satisfy a linear gradient condition, with $\partial u/\partial z = \partial v/\partial z = \partial w/\partial z = 0$.

The vortex ring is initialised as a Gaussian distribution of vorticity arranged around a ring centreline that is perturbed slightly from being perfectly circular, so that written in terms of the distance from the local position of the centreline $R'(\theta)$ we have

$$\omega_\theta = \frac{\Gamma}{\pi\delta^2}\, e^{-s^2/\delta^2} \tag{1}$$

where $s(\theta)^2 = z^2 + (r - R'(\theta))^2$. We suppose that the local radius $R'(\theta)$ can be written to include a small parameter $\varsigma = 0.0002$ multiplied by the sum of a set of $N$ Fourier modes, each with unit amplitude and random phase, so that

$$\begin{aligned} R'(\theta) &= R_0\,[1 + \varsigma f(\theta)] \\ f(\theta) &= \sum_{n=1}^{N} A_n \sin(n\theta) + B_n \sin(n\theta), \end{aligned}$$

where $A_n^2 + B_n^2 = 1$. Although this method leads naturally to a divergence-free velocity field, the continuity of the vortex lines themselves is not guaranteed – partly because the vorticity should be tilted slightly to follow the tangent to the path of the vortex centreline, and partly because the implied cross-section area of the vortex is not perfectly constant around the ring. The above vorticity field can be corrected to become divergence-free by superimposing the gradient of a scalar field $\nabla\phi$ and requiring that $\phi$ satisfy a Poisson equation whose source term is the divergence error of the original vorticity field. The complete initial field is then obtained by solving for the vector stream function that is consistent with the vorticity distribution, and the velocity field then follows directly by taking its curl.

Table 1: Part I run parameters

| Case | $\delta_0/R_0$ | $\Gamma_0/\nu$ | $L_x{\times}L_y{\times}L_z$ | $N_x{\times}N_y{\times}N_z$ |
|---|---|---|---|---|
| A | 0.413 | 5500 | $8R_0$x$8R_0$x$8R_0$ | 256×256×256 |
| B | 0.200 | 7500 | $8R_0$x$8R_0$x$8R_0$ | 512×512×512 |

We present results for a thick- (case A) and a thin-core (case B) vortex ring of initial radius $R_0$, initial core radius $\delta_0$ at a Reynolds number as defined by the initial ring circulation $\Gamma_0$ over kinematic viscosity $\nu$. The run parameters are documented in table 1, where $L$ is the domain length and $N$ is the number of grid cells.

### Free Surface Interaction

The free surface simulations use a similar second-order finite-difference discretisation but additionally allow for the surface to deform. One difference is that the pressure solver is replaced by a red-black successive over-relaxation (RB-SOR) method that incorporates the free surface boundary condition. The additional complexity of having a moving boundary that cuts through the cartesian grid is addressed using a split-merge technique. This is equivalent to the volume of fluid method, which accounts for the free surface geometry in a conservative manner, see Thomas *et al.* (1995) for details. The approach requires that the surface slope is less than the aspect ratio of the cell.

The domain dimensions and grid resolution are initially the same as used in case $A$ allowing us to either directly embed the vorticity field from the precursor simulation as the initial condition, or use the vorticity distribution from equation 1. The velocity field is subsequently derived from the vector potential associated with the vorticity field.

Due to the increasing ring diameter as it approaches and propagates near to the free surface, it becomes necessary to expand the domain horizontally. This is accompanied by a reduction in the vertical box length $L_z$ to approximately maintain the number of grid points. The velocity field is reconstructed by employing the above vorticity embedding method in the expanded domain. The expansion procedure is performed when the ring approaches within $2.5R_0$ of the edge of the domain.

Radial expansion is also accompanied by a thinning of the core requiring additional grid resolution. This is achieved by Fourier interpolation in the horizontal directions and a third order cubic spline in the vertical direction. The regriding is used to maintain a resolution corresponding to 18 grid cells spanning the core diameter.

The presence of the free surface introduces a Froude number $\mathrm{Fr} = \Gamma_0/\sqrt{gR_0^3}$, where $g$ is the acceleration due to gravity, which determines the magnitude of surface deformation. The choice of Froude numbers is restricted by the surface slope limit.

## RESULTS

## UNBOUNDED VORTEX RING

During the laminar phase the initially toroidal ring is deformed through the development of the azimuthal instability. The instability excites a narrow band of azimuthal waves with the dominant wave number $\widehat{m}$ at breakdown equal to 6 and 9 for cases $A$ and $B$ respectively, which agrees with

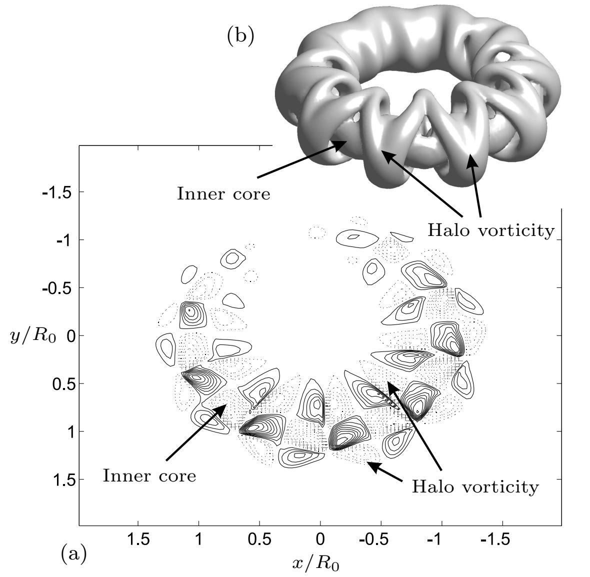


Figure 1: Visualisation of the secondary structure at time $t\Gamma_0/R_0^2 = 84.6$. (a) Contours of $\omega_z$ on the horizontal plane through the centre of ring ($z = 0$) for Case B: ———, $\omega_z > 0$; ⋯⋯, $\omega_z < 0$. Contour increments $|\omega_{z\ max}|/10$. (b) Isosurface of the second invariant II of the velocity gradient tensor, $\mathrm{II}R_0^4/\Gamma^2 = -0.005$, viewed from above.

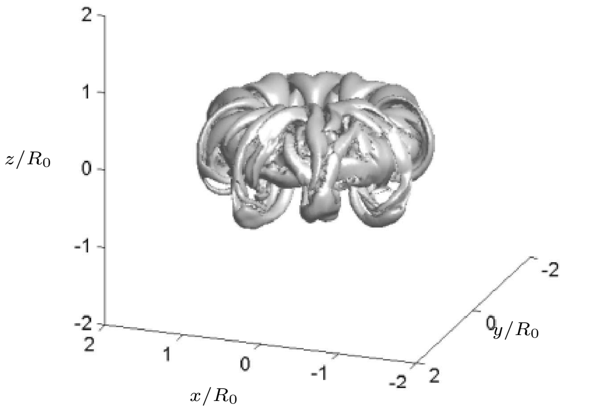


Figure 2: The generation of hairpin vortices. Isosurface of the second invariant of the velocity gradient tensor, $\mathrm{II}R_0^4/\Gamma^2 = -0.005$ for case B at time $t\Gamma_0/R_0^2 = 100.8$.

the theoretical predictions for a core with a Gaussian profile given by Shariff *et al.* (1994).

To aid understanding of the breakdown process we make a distinction between the region of intense vorticity at the core centre, which we call the "inner core", and the surrounding outer-core region of lower vorticity, which we call "halo" vorticity. (See the recent numerical study by Bergdorf *et al.* (2007) for a slightly different perspective on this topic.) The azimuthal instability causes displacement of both the inner vorticity (into a stationary wave pattern) and the halo vorticity. Where the inner core is displaced outwards the halo vorticity is displaced inwards and vice versa - consistent with the second radial mode (Widnall, 1975). The corresponding radial $\omega_R$ and axial $\omega_z$ vorticity components on a horizontal slice through the core have a three layer arrangement as shown in figure 1(a). The central layer corresponds to the inner core and the inner and outer layers to the halo vorticity. During the transitional phase the halo vorticity forms pairs of neighbouring loops of alternating signed vorticity, predominately of $\omega_R$ and $\omega_z$. These are products of tilting and stretching of the halo vorticity. The loops are disconnected from one another but touch at a saddle points in a radial plane aligned with the maximum inner core displacement but offset radially inward or outward in opposition to the inner core displacement. Two loops wrap around each azimuthal wave hence there are the same number of pairs of loops as waves around the azimuth of the core. The structure is visualised with an isosurface of the second invariant of the velocity gradient tensor in figure 1(b). An azimuthal decomposition of the modal behaviour shows a dominant $m = 1$ mode during the transitional phase, consistent with Dazin *et al.* (2006) and Shariff *et al.* (1994). This intermodulation product results in regions of preferential azimuthal wave growth, shown in figure 1.

As the azimuthal instability intensifies, the inner core and outer secondary structures are stretched, resulting in a peak in the total ring enstrophy. The stretched loops begin to protrude locally outside the entrainment bubble. They then become convected by the free stream flow and begin to trail behind the vortex ring. The loops originally developed as counter rotating pairs side by side, but as they trail outside of the ring the loops detach and reattach with their neighbour at the saddle point to form hairpin vortices that fill the wake (Figure 2). The localised equilibrium between the inner core and the outer halo vorticity is broken, as the halo vorticity leaves the entrainment bubble and the core becomes locally turbulent at the position of the initial hairpin vortex shedding. The azimuthal instability wave was not found to rotate prior to the ring becoming turbulent, which conflicts with the interpretation of Maxworthy (1977). The waves continue to develop across the remainder of the ring, unhindered until the secondary structure is shed into hairpin vortices around the entire azimuth of the ring, and the ring can be considered to be fully turbulent.

The stationary coherent vortical structure which mark the transitional phase is superseded by the swirling of vorticity filaments around an instantaneous origin. Figure 3(a) shows that the core region of case A breaks down into a number of interwoven vortex filaments. No well-defined coherent core persists and circulation is shed via a continual stream of vortex filaments into the wake. The thin-core ring (case B) however maintains a core region of concentrated vorticity (the dark region in Figure 3(b)) which is consistent with the turbulent visualisations of Wiegand & Gharib (1994). The core region is no longer stationary, but bends and twists with time. Vorticity filaments, similar to the secondary structure, are continually generated, wrapping and circulating around the turbulent core. Figure 3(b) shows a number of these vorticity filaments wrapped round the core region with long tails that trail into the wake and out of the domain, in agreement with Bergdorf *et al.* (2007). Just as for the thick-core ring, these vorticity filaments circulate around the core and gradually pass out of the vortex and into the wake as a stream of vorticity filaments and hairpin vortices, as visualised by Glezer & Coles (1990) and Wiegand & Gharib (1994). The ring was not simulated further into the turbulent regime. However an initial staircase-like decay of circulation, as reported by Wiegand & Gharib (1994) and Bergdorf *et al.* (2007), was noted.

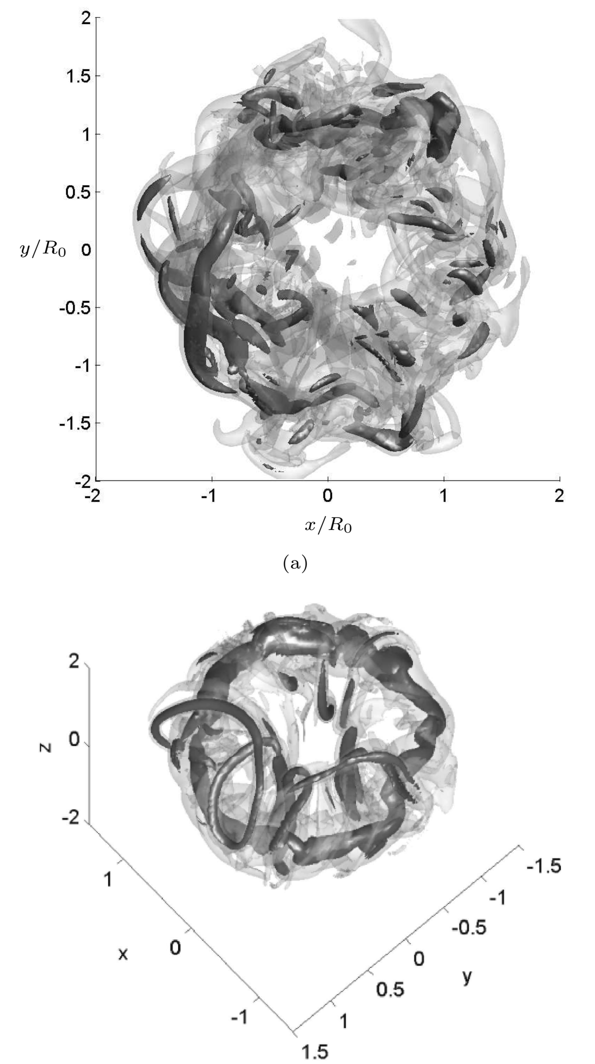


(a)

(b)

Figure 3: Double isosurface of vorticity magnitude $|\omega|$ for turbulent vortex rings. (a) Case A at time $t\Gamma_0/R_0^2 = 220$: dark surface level $|\omega|R_0^2/\Gamma_0 = 1.4$; translucent light surface level $|\omega|R_0^2/\Gamma_0 = 0.7$. (b) Case B at time $t\Gamma_0/R_0^2 = 136.8$: dark surface level $|\omega|R_0^2/\Gamma_0 = 2.5$; translucent light surface level $|\omega|R_0^2/\Gamma_0 = 1.25$.

## FREE SURFACE INTERACTION

The following results should be viewed as preliminary with current simulations employing a larger number of grid cells to improve the resolution of the vortex structure underway at the time of writing. These will be presented during the symposium.

### Laminar Ring

The free surface code was validated by comparing the simulation of a laminar ring propagating normally (90°) toward a free surface with the experimental results of Song *et al.* (1992). A laminar ring was initialised at depth $4R_0$, with $\delta_0/R_0 = 0.2$, $R = 1.0$, Re = 10000 and Fr = 0.252, which matches the parameters of their first test case, albeit with a slightly lower Reynolds (Song *et al.* used Re = 15100). The effect of lowering the Reynolds number for a laminar ring is to decrease the growth rate of the azimuthal

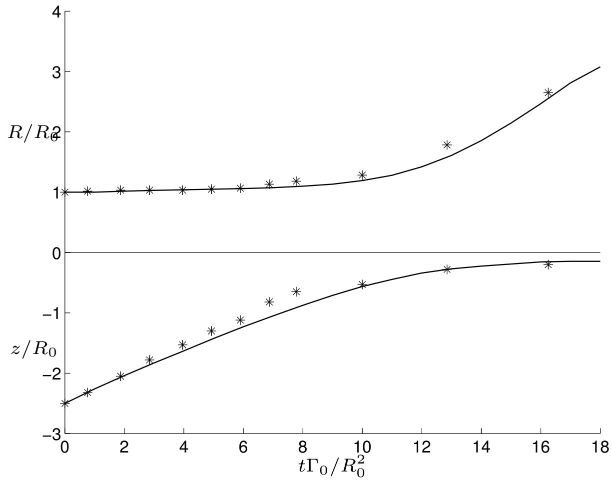


Figure 4: Comparison of vortex ring depth and radial expansion between DNS ——— and experiments ($***$) Song *et al.* (1992).

instability and increase core diffusion, but since the timescale for the surface interaction is relatively small neither is effected greatly. The evolution of the radial expansion and depth of the ring show excellent agreement with the experiments (figure 4). The approach of the ring induces a circular bulge on the surface above the ring, which grows as the ring draws closer. At a depth of about one initial radius $R_0$ the ring begins to expand, causing the surface bulge to fall and a circular surface depression to propagate outboard of the expanding ring, which is consistent with the observations of Song *et al.* (1992). After the last experimental reading documented in figure 4, the vortex ring continues to propagate under the surface for a further radial expansion of $1.5R_0$, at which point the ring disconnects and reconnects with the surface. The radial expansion was not recorded by Song *et al.* as far as the surface reconnection, as the errors in the employed video recording method became too large.

### Transitional Ring

The vorticity field for the thick-core ring (case A) was extracted and embedded $4R_0$ below the free surface, with the Froude number for the simulation set to 0.252. At the time of embedding, the ring had evolved for $130R_0^2/\Gamma_0$ time units and was in the transitional phase documented above, with a clearly defined wavy inner core distortion and associated secondary peripheral structure. As the ring approaches from $4R_0$ to $1R_0$ of the free surface the wavy core and secondary structure continue to develop and stretch, however a fully turbulent state is not reached. During this time the surface above the ring is again deformed into a bulge, however whereas the laminar surface bulge was circular, the transitional surface bulge was modulated by the stationary core wave pattern of the ring. As it moves to within a depth of $1R_0$, the presence of the surface begins to stabilise the ring. The growth of the inner core wave and associated secondary structure is suppressed. The shedding of the secondary structure was found to be a trigger for turbulence, however this does not occur and the ring remains in a transitional state. As for the laminar case, the radial expansion and subsequent propagation at a small depth induces an outboard depression on the surface. The depression is no longer circular but matches the wavy inner core pattern in shape, as shown by the dark region in figure 5(a).

At time $t\Gamma_0/R_0^2 = 29.6$ the ring is at depth order $\delta_0$, with

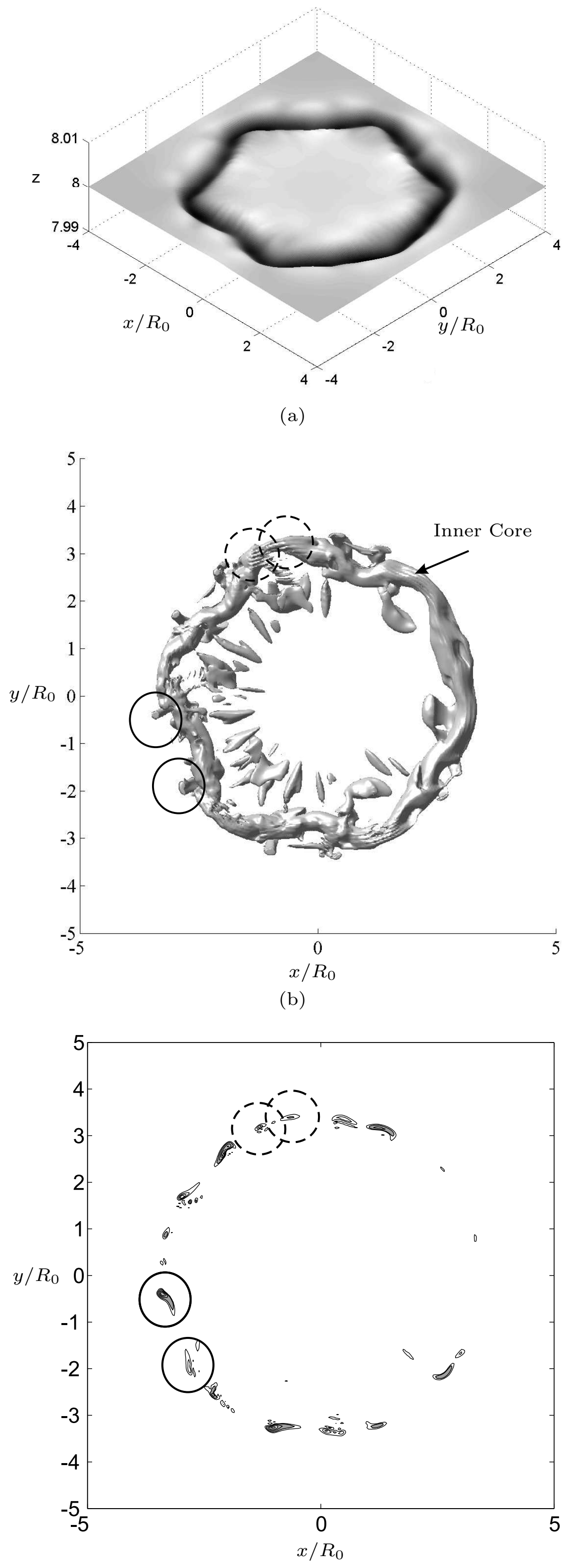


Figure 5: Transitional ring interaction with a free surface at time $t\Gamma_0/R_0^2 = 40.0$: (a) Surface distortion: light shading corresponds to elevation; dark to depression. (b) Vorticity structure below the surface visualised by isosurfaces of II, level $\mathrm{II}R_0^4/\Gamma^2 = -0.005$. (c) Surface normal vorticity $\omega_s$ at the free surface, contour increments $0.2 \times \omega_S^{max}$.

radius $1.5R_0$. The secondary loops of halo vorticity begin to come in contact with the surface. The loops disconnect and reattach to the surface just outboard of the inner core. This forms U-shaped vorticity tubes which encircle the inner core. As the inner core expands radially, it displaces the U-shaped tube with it. Two examples of the outboard attachment points of two separate U-tubes are highlighted by the solid circles in figure 5(b). The corresponding regions of surface normal vorticity $\omega_s$ at the free surface are shown with solid line circles in figure 5(c). The vortical structures inboard of the inner core in figure 5(c) are remnants of the secondary loops that remain disconnected to the ring at the surface. The secondary structure develops as neighbouring loops of counter-rotating vorticity, hence the corresponding neighbouring regions of $\omega_s$ are of opposing sign. This type of surface reconnection is different to that described by Song *et al.* (1992), who considered the laminar surface reconnection of the inner core region. The laminar rings they investigated had not aged enough to develop the secondary structure, hence a sinusoidal wave that develops on the inner core region due to a Crow-type instability (Crow, 1970) which causes it to reconnect with the free surface.

At time $t\Gamma_0/R_0^2 = 36.0$ the inner core begins to interact with surface. The inner core is distorted into a stationary wave at 45° to the vertical, hence isolated wave crests become in close contact to the the surface. The inner core begins to disconnect and reconnect to the surface at these locations, as indicated by the dashed circles in figure 5(b). The resultant $\omega_s$ generated by the reconnection to the surface is indicated in figure 5(c) by corresponding dashed circles. The two neighbouring vorticity contours are of opposite sign, consistent with the connection of two separate filaments.

The final stages of the interaction are currently under investigation to determine if the inner core detaches around the entire azimuth to form a series of U-shaped hoops, as do the laminar rings of Song *et al.* (1992).

#### Turbulent Ring

A thick-core ring was extracted from case A and embedded $4R_0$ below the surface, with the Froude number for the simulation set to 0.252. At the time of embedding, the ring had evolved for $159.3R_0^2/\Gamma_0$ time units which is $10R_0^2/\Gamma_0$ before the onset of turbulence. As the ring travels toward the surface it becomes turbulent, shedding the secondary loops as a string of hairpin vortices which trail behind the turbulent core as shown in figure 6. The approach of the turbulent ring to the surface induces a bulge on the surface, but with no clear pattern, in contrast to the transitional and laminar cases. The structure of the core was shown above to be a swirling mass of intertwined vorticity filaments. As turbulent ring moves closer to the surface the swirling vorticity filaments come in close contact to the surface inboard of the vortex core. As they rotate around the core underneath the surface, the filaments connect to the surface and remain connected in the outer periphery of the turbulent ring as it expands radially. As the ring expands, more and more filaments reconnect with the surface.

### SUMMARY

Using DNS we have examined the three different stages of unbounded vortex ring evolution, laminar, transitional and turbulent, and the corresponding vortical structures. Laminar rings consist of a toroidal core region and are susceptible to the azimuthal instability. Transitional rings have

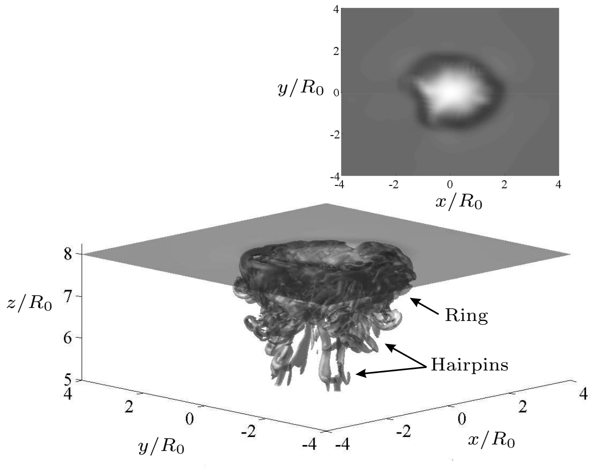


Figure 6: Turbulent ring surface interaction featuring a translucent free surface at time $t = 31.2\Gamma_0/R_0^2$. Vorticity structure below the surface is visualised by isosurfaces of II, with level II = -0.005. The free surface distortion pattern is shown in the insert with light shading corresponding to regions of elevation and dark to depression.

a wavy inner core region which is encompassed by a mesh of loops of halo vorticity. Neighbouring loops are of opposing sign vorticity and their shedding from the ring heralds the onset of turbulence. The structure of the turbulent ring depends on the relative core thickness with thin rings maintaining a coherent core region and thick-core rings typified by a swirling mass of vorticity filaments. We have also studied how each of the structures interact with a deformable surface, and their characteristic surface deformation and reconnection patterns. Future work will investigate how the rings affect and are affected by a free surface containing pre-existing plane gravity waves

## ACKNOWLEDGMENTS


This research was funded jointly by the UK Engineering and Physical Sciences Research Council (EPSRC) and the Defence Science and Technology Laboratory (Grant GR/S82299/01) with Dr R P Hornby as contract monitor. Computational resources were provided by EPSRC and the UK Turbulence Consortium. Special thanks go to Dr J.A. Redford and Dr K Shariff for their support, encouragement and expertise.


## REFERENCES


Ashurst,W.T., and Meiron, D.I., 1987, "Numerical Study of Vortex Reconnection", *Physical Review Letters*, Vol. 58, pp. 1632-1635.

Bergdorf, M., Koumoutsakos, P., and Leonard, A., 2007, "Direct Numerical Simulation of Vortex Rings at $\mathrm{Re}_\Gamma = 7500$", *Journal of Fluid Mechanics*, Vol. 581, pp. 495-505.

Crow, S.C., 1970, "Stability Theory for a Pair of Trailing Vortices", *AIAA*, Vol. 8, pp. 2172-2179.

Dazin, A., Dupont, P. and Stanislas, M., 2006, "Experimental Characterization of the Instability of the Vortex Ring. Part II: Non-Linear Phase.", *Experiments in Fluids*, Vol. 41, pp. 401-413.

Glezer, A., and Coles, D., 1990, "An Experimental Study of a Turbulent Vortex Ring", *Journal of Fluid Mechanics*, Vol. 211, pp. 243-283.

Kerswell, R.R., 2002, "Elliptical Instability" *Annual Review of Fluid Mechanics*, Vol. 34, pp. 83-113.

Krutzsch, C.H., 1939, "Über eine Experimentell Beobachtete Erscheining an Werbelringen bei Ehrer Translatorischen Beivegung in Weklechin, Flussigheiter", *Annln. Phys.*, Vol. 5, pp. 497-523.

Maxworthy, T., 1972, "The Structure and Stability of Vortex Rings", *Journal of Fluid Mechanics*, Vol. 51, pp. 15-32.

Maxworthy, T., 1977, "Some Experimental Studies of Vortex Rings", *Journal of Fluid Mechanics*, Vol. 81, pp. 465-495.

Naitoh, T., Fukuda, N., Gotoh, T., Yamada, H. and Nakajima, K., 2002, "Experimental Study of Axial Flow in a Vortex Ring", *Physics of Fluids*, Vol. 14, pp. 143-149.

Quyuan, Y. and Chu, C.K., 1997, "The Nonlinear Interaction of Vortex Rings with a Free Surface", *Acta Meccanica Sinicia*, Vol. 13, pp. 120-129.

Schneider, P., 1980, "Sekundärwirbelbildung bei Ringwirbeln und in Freistrahlen" *Z. Flugwiss. Weltraumforsch*, Vol. 4, pp. 307-318.

Shariff, K., Verzicco, R., and Orlandi, P., 1994, "A Numerical Study of Three-Dimensional Vortex Ring Instabilities: Viscous Corrections and Early Nonlinear Stage", *Journal of Fluid Mechanics*, Vol. 279, pp. 351-375.

Song, M., Bernal, L.P., and Tryggvason, G., 1992, "Head-on Collision of a Large Vortex Ring with a Free Surface", Vol. 4, pp. 1457-1466.

Thomas, T.G., Leslie, D.C., and Williams, J.J.R., 1995, "Free Surface Simulations Using a Conservative 3d Code", *Journal of Computational Physics*, Vol. 116, pp. 52-68.

Widnall, S.E., and Sullivan, J.P., 1973, "On the Stability of Vortex Rings", *Proc. R. Soc. London. A*, Vol. 332, pp. 335-353.

Widnall, S.E., 1975, "The Structure and Dynamics of Vortex Filaments", *Annu. Rev. Fluid Mech.*, Vol. 7, pp. 141-165.

Widnall, S.E., and Tsai, C-Y., 1977, "The Instability of the Thin Vortex Ring of Constant Vorticity", *Phil. Trans. R. Soc. Lond.*, Vol. 287, pp. 273-305.

Wiegand, A., and Gharib, M., 1994, "On the Decay of a Turbulent Vortex Ring", *Physics of Fluids*, Vol. 38, pp. 3806-3808.

Yao, Y.F., Thomas, T.G., Sandham, N.D., and Williams, J.J.R., 2001, "Direct Numerical Simulation of Turbulent Flow Over a Rectangular Trailing Edge", *Theoretical and Computational Fluid Dynamics*, Vol. 14, pp. 337-358.